buildings

MDPI

Article

A Moment-Rotation Model of Semi-Rigid Steel Structure Joints with Bolted Connection

Mengxin Kang [1,*], Shifeng Hou [2], Juyang Cai [1] and Liang Zhang [3]

[1] School of Civil Engineering and Architecture, Northeast Electric Power University, Jilin City 132012, China; 2202400965@neepu.edu.cn
[2] Heyuan Power Supply Bureau, Guangdong Power Grid Co., Ltd., Heyuan City 517000, China; 3228167586@gd.csg.cn
[3] Economic and Technical Research Institute of State Grid Henan Electric Power Company, Zhengzhou 450052, China; zhangliang13@ha.sgcc.com.cn
* Correspondence: linxizimin@163.com

Abstract

ANSYS software was used to analyze the moment-rotation relationship of semi-rigid steel structure joints with bolted connection. A parametric study was conducted to examine the influence of eight key variables—including bolt number, bolt grade, angle steel grade, bolt diameter, angle steel thickness, angle steel width, preload magnitude, and friction coefficient—on the bending behavior of semi-rigid joints with bolted connection. Parametric analysis reveals that the initial rotational stiffness is most significantly influenced by the bolt diameter, the width and thickness of the angle steel, the bolt preload, the coefficient of friction, and the bolt number. The stiffness exhibited an average increase of 50.6% for every 4 mm increment in bolt diameter from 12 mm to 24 mm. Expanding the angle steel width from 50 mm to 75 mm resulted in a substantial 88.5% average increase in stiffness, while a further width increase from 75 mm to 110 mm led to a smaller average increase of 17.4% per 17.5 mm. Similarly, the stiffness rose by an average of 33.8% for every 2 mm increase in the thickness of the angle steel within the 4 mm to 10 mm range. A 25% increase in bolt preload correlated with a modest average stiffness gain of 2.7%. The rate of stiffness improvement diminished with increasing friction coefficient. In contrast, the initial rotational stiffness exhibited a relationship that is approximately linear with respect to the quantity of bolts. Regarding the ultimate bending moment, the key influencing factors were identified as bolt diameter, preload, coefficient of friction, and number of bolts. The ultimate moment demonstrated a non-monotonic relationship with bolt diameter, characterized by an initial increase, followed by a decrease, and then a sharp subsequent rise. Linear enhancements in the ultimate moment were observed with increases in both bolt preload and coefficient of friction. Furthermore, the ultimate bending moment showed a gradual increase with the number of bolts. Based on the results, a bending moment-rotation curve model of joints with bolted connection is established, and the expression of each parameter in the model is calculated. This model can be applied to simulation of the bending performance of semi-rigid joints with bolted connection.

Keywords: semi-rigid joints; initial rotational stiffness; ultimate bending moment; moment-rotation model

Check for updates

Academic Editor: Hiroshi Tagawa

Received: 17 October 2025
Revised: 19 December 2025
Accepted: 25 December 2025
Published: 1 January 2026

Copyright: © 2026 by the authors. Licensee MDPI, Basel, Switzerland. This article is an open access article distributed under the terms and conditions of the Creative Commons Attribution (CC BY) license.

1. Introduction

Semi-rigid connections, which are a connection form between hinged and fully rigid connections, are a primary form of connection in steel structures [1]. These connections offer advantages such as enhanced structural seismic performance, straightforward fabrication, and ease of installation, making them widely applicable in prefabricated construction. However, their complex mechanical behavior presents significant challenges for theoretical analysis. Chen et al. [2] established an experimental database of semi-rigid steel beam-column joints. Based on the steel structure connection database program, the bending moment and rotational angle characteristics of different types of connections were analyzed and determined, and the corresponding curve models were given. Attiogbe et al. [3] used the Richard-Abbott and Ramberg-Osgood functions to fit the experimental moment-rotation data with the least square method. The comparison showed that the Richard-Abbott function provided a more accurate fit than the Ramberg-Osgood function, and a multiple regression analysis method for deriving the standard connection moment-rotation function from all available experimental data was described. Attarnejada et al. [4] carried out vibration analysis of a semi-rigid frame, considering joint bending moment and shear force. The numerical model of the semi-rigid frame was established by nonlinear finite element method. Thai et al. [5] proposed an accurate and effective numerical method to calculate the reliability of a semi-rigid connection steel frame system. The nonlinear characteristics of the semi-rigid connection can be represented by a three-parameter power function model. Yu et al. [6] put forward a numerical method for dynamic collapse analysis of steel frames with semi-rigid connection based on the finite element method. Zhao et al. [7] developed a finite element model of a branch plate-circular tube joint, and subsequently a semi-rigid model of the joint, including seven parameters. Mokhtar et al. [8] studied the behavior of precast concrete beam-to-column connections with partly hidden corbels through full-scale tests under static and reversible loads. The moment resistance, failure mechanisms, and moment-rotation (M-ϕ) responses were evaluated. By combining M-ϕ data with the beam line method and fixity factor, the proposed connection (BHC2) was classified as semi-rigid with medium strength (Zone III), confirming its suitability for semi-rigid frame analysis. Ding et al. [9] performed semi-rigid analysis of a rigid frame structure, discussed the feasibility of using linear model analysis, analyzed the influence of semi-rigid joints on the stress and deformation of rigid frame structures, and described design criteria for steel frame structures. Ma et al. [10] investigated a novel semi-rigid HCR joint system for single-layer reticulated steel (SRS) cooling towers. A validated finite element model of the joint was used to analyze its behavior under various loading combinations. The obtained moment-rotation curves were then incorporated into structural stability analyses of full cooling towers. The research evaluated the influence of joint stiffness, structural height, and grid size on the buckling mode of the structure, comparing models with uniform and location-specific joint stiffness. Celik [11] reviewed the historical development and current state of research on semi-rigid connections in steel frames. Their study highlights the gap between theoretical recognition of semi-rigid behavior and its practical application. The study systematically categorizes joint modeling methods into seven types and expands the scope beyond moment-rotation to include other load effects and connection types. The aim was to facilitate broader practical adoption by synthesizing analysis methods and design approaches. Pan et al. [12] carried out a sensitivity analysis of a composite frame structure, considering the correlation of the geometric parameters of the joints, and calculated the moment-rotation curve, considering the geometric parameters. Considering the influence of the semi-rigidity of the joints, a solid model and a multi-scale model were established, and a time history analysis in response to typical seismic waves was carried out. Kang et al. [13] conducted a static experimental study on the mechanical properties of semi-

rigid beam-column joints with T-stub connections. A finite element model was proposed to conduct a parametric investigation of factors influencing the semi-rigidity of the joints. A mathematical expression of the moment-rotation model of the joints was obtained by regression analysis. Zhai et al. [14] developed theoretical expressions for the initial lateral stiffness of semi-rigidly connected plate-type modular frame structures utilizing a modified displacement method. The theoretical results demonstrated strong consistency with both experimental measurements and finite element method (FEM) analyses. Nguyen et al. [15] introduced an innovative approach for analyzing steel frames incorporating semi-rigid connections and displacement constraints, utilizing a condensed finite element formulation. Qiu et al. [16] analyzed the moment-rotation curve of typical steel tower joints by finite element simulation and developed a computational approach for determining single-angle stability bearing capacity by incorporating initial imperfections and residual stresses through the application of spring elements. Tang et al. [17] addressed the semi-rigid behavior of bolted tube-gusset K-joints in steel tubular transmission towers, which are currently idealized as purely pinned or rigid in design codes. A direct prediction method using a Support Vector Regression model was proposed to accurately predict the moment-rotation curves of these joints. Validated against finite element data and other models, the SVR-based method demonstrates superior accuracy and reliability, providing a valuable tool for engineering analysis and design. Tang et al. [18] developed a predictive methodology aimed at accurately estimating stability and bearing capacity, while effectively quantifying associated uncertainties. Tang et al. [19] proposed a reliability evaluation framework for steel tubular transmission towers with semi-rigid bolted connections (STTTs-SRCs) that accounts for uncertainties in dimensions, materials, connections, and stochastic wind loads. The results demonstrate that semi-rigid connections significantly influence both component-level and global failure probabilities for stress-related failure modes. Al-Sherif et al. [20] investigated the effect of beam-column connection with semi-rigid rotational stiffness on the behavior of different frame cases. The results showed that the semi-rigidity of beam-column connections make the maximum vertical displacement, horizontal displacement, and maximum rotation significantly increase, and the load-displacement curve of the frame structure is less stiff. Tang et al. [21] investigated the influence of semi-rigid connections on the stability and capacity of cross-bracings in steel tubular transmission towers. A hybrid PSO-BPNN model was developed to predict the bearing capacity and facilitate probabilistic assessment. Using a dataset of 7425 FE-generated samples, the model demonstrates high accuracy. The results show that semi-rigid connections significantly enhance the stability, bearing capacity, and structural reliability of the cross-bracings.

Current research on moment-rotation curve models for bolted connections in transmission towers remains limited in terms of considered parameters, and there is a notable absence of an accurate model capable of reliably characterizing moment-rotation behavior in finite element simulations of high-voltage transmission tower joints. To address this gap, this study develops a validated finite element model of a bolted main member bar connection for transmission towers. Using this model, the semi-rigid behavior of the connection is systematically investigated by analyzing eight key parameters: the number of bolts, bolt grade, angle steel grade, bolt diameter, angle steel thickness, angle steel width, preload force, and friction coefficient. Based on the results, a generalized moment-rotation model that incorporates these influential parameters is formulated, providing a more reliable basis for the simulation of such structural connections.

2. Finite Element Model

2.1. Geometric Model

In this paper, the common bolted connection joints in transmission towers are used as the research object. In semi-rigid research, bolted connection joints are divided into non-plate joints and plate joints. Non-plate joints are composed of main members and auxiliary members, and the two angle steels are connected by bolts. In plate joints, the main members and auxiliary members are connected by the joint plate, which is similarly connected by bolts. A geometric model is shown in Figure 1, where bolt diameter is d, angle steel width is l, and angle steel thickness is h.

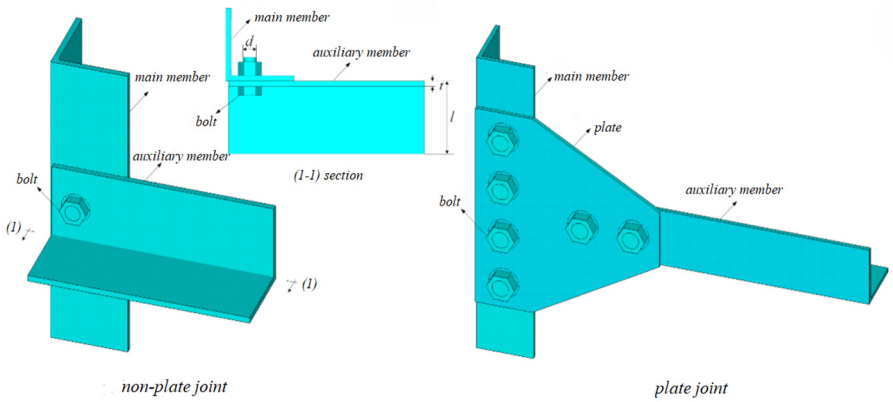

Figure 1. Bolted connection joint geometric model.

2.2. Finite Element Modeling Procedure

In this paper, ANSYS 17.2 software was used for finite element analysis. In the finite element model, the solid structure adopts a SOLID186 element, which includes angle steels, bolts, and plate. The contact pair is modeled using the TARGE170 and CONTA174 elements, while the preload is applied through the PRETS179 element. The contact element is positioned over the solid element and is in quasi-contact with the target surface element. The contact interaction is activated by penetration of the contact element beyond a target surface. By setting key parameters and real constant values, such as the normal contact stiffness FKN and the contact penetration tolerance factor FTOLN, the properties of the contact pair element can be adjusted to conform to the actual situation.

To accurately capture their elastoplastic response, the material stress-strain relationship was defined by an MISO model, characterized by a three-stage curve: an elastic slope of E, followed by a yield plateau and a plastic strain-hardening slope of 0.02E, as illustrated in Figure 2.

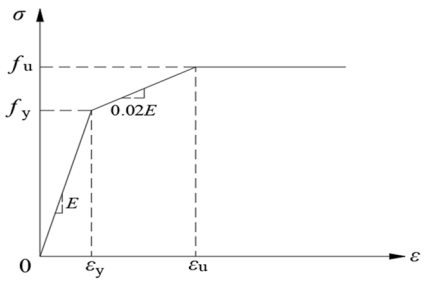

Figure 2. Stress-strain curve model of the material.

The contact interactions in the bolted joint model were modeled using contact pairs defined between surfaces sharing the same real constant. Four such pairs were established: between the main member and nut, the main and auxiliary members (plate), the auxil-

iary member and nut, and the bolt shank and the bolt holes. Contact parameters were determined by correlating numerical results with experimental data. Bolt preload was applied via pre-tension elements to clamp the angle steel, thereby preventing slip under load. A 10 mm long loading segment was extended from the angle steel end, and a force was applied perpendicularly to its lower surface to simulate a moment load while avoiding excessive stress concentration; the overall setup is illustrated in Figure 3.

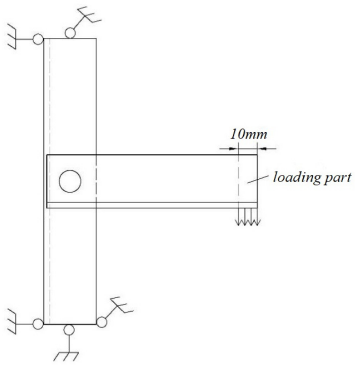

Figure 3. Constraints and loading settings for bolted connection joints.

2.3. Finite Element Model Validation

The experimental results of three typical joints are introduced in reference [22], and joints A and C are joints without plates and with plates, respectively, representing two typical joint types in transmission tower structures. The typical joints A and C in the experiment [22] are used as references to establish bolted connection joint models without plates and with plates, as shown in Figure 4. The angle steel material is Q235B, the bolt is a 4.8-grade galvanized rough bolt, and the friction coefficient of the galvanized surface is 0.19.



(**a**) Joint without plate



(**b**) Joint with plate

Figure 4. Physical diagrams of typical joints.

The joint A model without plates is established, as shown in the Figure 5. Mesh generation affects the accuracy of the solution, and the joint A model use mesh division accuracies of 1 mm, 2 mm, 3 mm, and 4 mm. Loads were applied to the model, the analysis was performed, and the rotational stiffness and bending moment load of the joints were obtained by analyzing the resulting data.

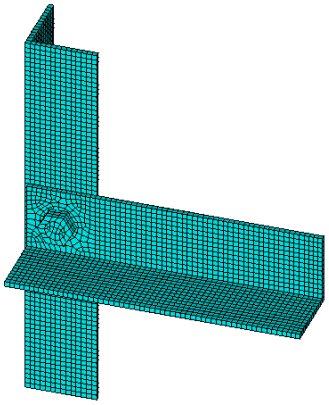

Figure 5. Joint A model without plates.

A comparison of the finite element model solution results and time under different mesh generation accuracies is shown in Table 1. As the mesh division becomes more accurate, the finite element solution results tend to be stable, but the solution time becomes longer. Taking into account the mesh sensitivity and the solution time, 4 mm was selected as the most accurate model mesh division.

Table 1. Comparison of solution results and times with different mesh accuracies.

Mesh Size (mm)	Rotational Stiffness (rad)	Bending Moment (kN × m)	Time (min)
2	40.891	0.088	521
3	40.85788	0.088	210
4	40.65306	0.088	11
5	36.9529	0.088	7
6	35.14845	0.086	5

The main algorithms applicable to contact analysis currently are the augmented Lagrangian, penalty function, multipoint constraint (MPC), Lagrange multiplier on contact normal and penalty on tangent (composite method), and pure Lagrange multiplier on contact normal and tangent algorithms. Different contact algorithms were employed to analyze the typical joint A model, and the results were analyzed to select the appropriate algorithm. The MPC approach is only suitable for certain bonded or no-separation contact, and not for separation contact in a bolted joint model; the composite method had poor stability and longer iteration time in the load step; the pure Lagrange multiplier algorithm has a long iteration time at the end of the linear stage in the rotation process, resulting in convergence failure; and the augmented Lagrangian and penalty function algorithms show good stability and convergence in the solution process. Considered comprehensively, the augmented Lagrangian algorithm was chosen as the contact analysis algorithm.

Different real constant values of contact pairs were used to determine the characteristics of contact behavior, including normal contact stiffness FKN, contact penetration tolerance factor FTOLN, and tangential contact stiffness FKT. Taking the typical joint A model as the analysis object, different real constant values of the contact units were set, loads were applied, and the model was solved. The influence of different real constants on the mechanical properties of the joint models was analyzed, and the finite element results were compared with the experimental results. When the normal contact stiffness FKN is 2500 GPa/m, the contact penetration tolerance factor FTOLN is 0.1, and the tangential contact stiffness factor FKT is 1.4; the load-displacement curve of the numerical model is in good agreement, as shown in Figure 6. The displacement nephogram of typical joins

A and C obtained by finite element simulation is shown in Figure 7, demonstrating good agreement with experimental results.

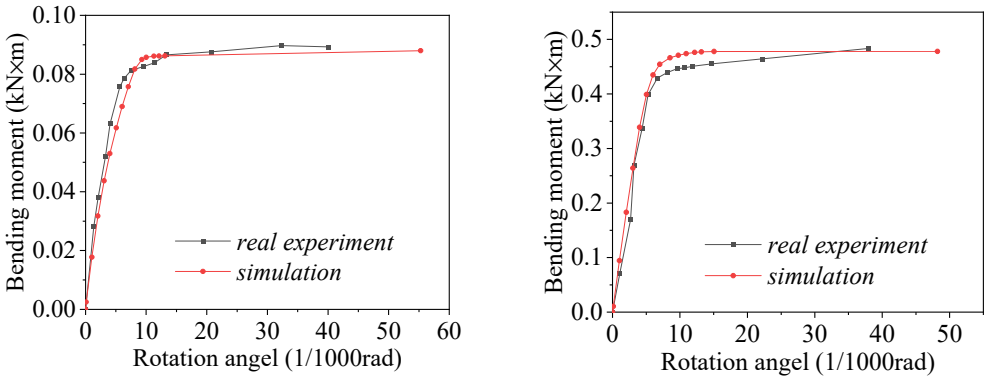

(**a**) Type A joint without plate (**b**) Type C joint with plate

Figure 6. Experimental curve and finite element simulation curve.

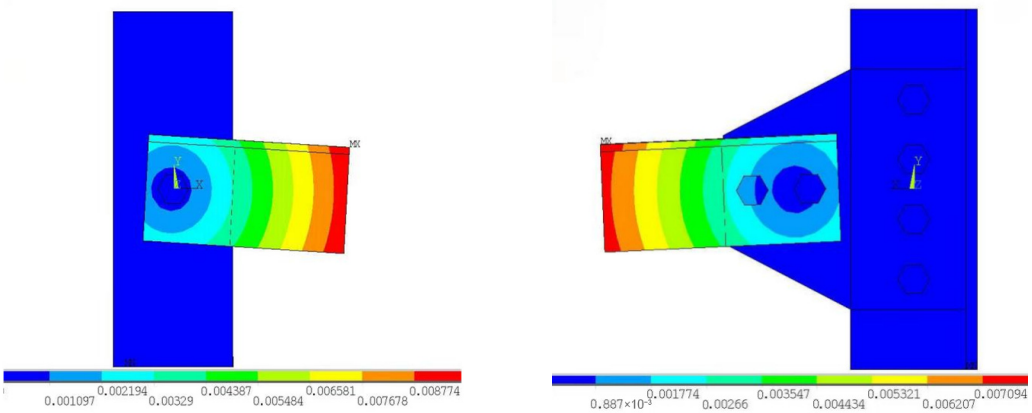

(**a**) Joint without plate (**b**) Joint with plate

Figure 7. Model displacement nephogram of typical joints.

The load-displacement curves exhibited few differences in initial stage and turning point. The material utilizes a simplified constitutive model based on its strength grade, and there are computational errors in the numerical simulation, which contribute to the result errors. However, the errors are within the acceptable range, and the finite element simulation is effective. So far, the bending moment rotation experiments of two independent bolted joints have been restored, so the finite element model of bolted joints can be used to simulate the bending moment-rotation process of the joints for the semi-rigidity analysis.

2.4. Parameter Settings for Bolted Connection Main Member Joints

To analyze the semi-rigidity of the bolted joint model, eight influencing factors are considered in this paper, including the number of bolts n (this includes the quantity of bolts (n_0)), the grade of the bolts, the grade of the angle steel, the diameter of the bolts (d), the thickness of the angle steel (t), the width of the angle steel (l), and the preload applied to the bolts (relative to the installation), and the friction coefficient. The values of each influencing factor are shown in Table 2. A total of 72 sets of contrast tests were set up, considering different influencing factors.

Table 2. Values of factors influencing the bolted joint.

Model-Influencing Factors	Values
Number of bolts n_0	4, 3, 2, 1
Bolt grade (grade)	8.8, 6.8, 5.8, 4.8
Angle steel grade (grade)	Q235, Q345, Q390, Q420
(EN 10027-1:2016) [23]	(S235JR, S335JR, S390JR, S420NL)
Bolt diameter d (mm)	24, 20, 16, 12
Angle steel thickness t (mm)	10, 8, 6, 4
Angle steel width l (mm)	110, 90, 75, 50
Bolt preload (relative to the installation) x%	100%, 75%, 50%, 25%
Friction coefficient μ	0.5, 0.4, 0.3, 0.2, 0.1

3. Results and Analysis

The bending moment-rotation relationship of the bolted joint model, derived from the numerical analysis results, is presented in Figure 8. The overall response exhibits a trilinear characteristic, comprising linear, nonlinear, and hardening stages. Initially, under monotonic static loading, the moment increases linearly with the rotation angle. Upon reaching the yield moment, the relationship transitions into a nonlinear phase. During the subsequent phase of loading, due to the rapid expansion of the plastic zone, a slight increase in moment leads to considerable growth in rotation, indicating that the joint approaches its ultimate state. The obtained numerical curve aligns well with the moment-rotation behavior recommended by current Chinese and European steel structure design codes [24,25].

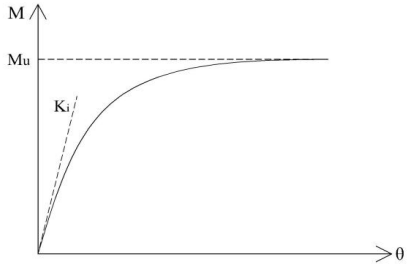

Figure 8. Bending moment rotation curve of the bolted connection joint model.

3.1. Factors Influencing Initial Rotation Stiffness

3.1.1. Bolt Diameter

Next, 31 comparative tests were designed to evaluate the influence of bolt diameter on the initial rotational stiffness, with the results summarized in Figure 9. For a single-bolt configuration, as the bolt diameter increased from 12 mm to 24 mm, the initial rotational stiffness rose by an average of 64.7%, 47.3%, and 49.5% per 4 mm increment under different angle steel thicknesses, yielding an overall average increase of 53.8%.

For the two-bolt configuration, the rotational stiffness exhibited a substantial increase with bolt diameter. As the diameter was increased from 12 mm to 20 mm, the stiffness increased by an average of 62.3% and 37.5% per 4 mm increment under varying angle steel widths. A further diameter increase to 24 mm yielded an average stiffness growth of 42.3% for angle steel widths between 75 mm and 110 mm. Overall, a 4 mm increase in bolt diameter across the 12 mm to 24 mm range produced an average stiffness enhancement of 47.3%.

Combining all cases with different angle steel thicknesses and widths, each 4 mm increase in bolt diameter resulted in an average stiffness enhancement of 50.6%. These results indicate that bolt diameter significantly affects initial rotational stiffness, with the

magnitude of this effect being notably influenced by the thickness and width. This behavior can be attributed to the increased contact area with larger diameters, which enhances the frictional resistance at the interface and thereby improves initial rotational stiffness.

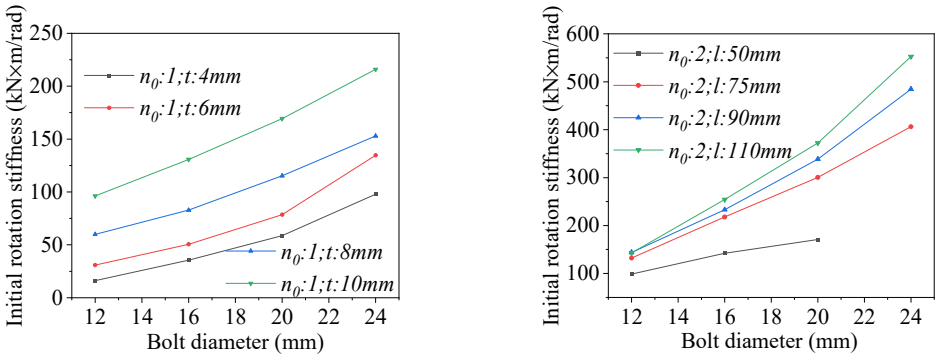

(**a**) Angle steel thickness (**b**) Angle steel width

Figure 9. Effect of bolt diameter on initial rotation stiffness.

3.1.2. Angle Steel Size

To investigate the effect of angle steel dimensions on initial rotational stiffness, 16 comparative tests were conducted, with the results summarized in Figure 10. For a three-bolt configuration, increasing the width from 50 to 110 mm resulted in an average enhancement in stiffness of 88.5% when the width expanded from 50 mm to 75 mm. In the range of 75 mm to 110 mm, each 17.5 mm width increase led to an average increase in stiffness of 17.4%. These results indicate that, while wider-angle steel enhances initial rotational stiffness, the rate of improvement diminishes as the width increases. This phenomenon is ascribed to the expanded contact surface area between the bolt and the angle steel, which strengthens frictional resistance. However, beyond a certain width, the influence of further contact area expansion on stiffness becomes less pronounced.

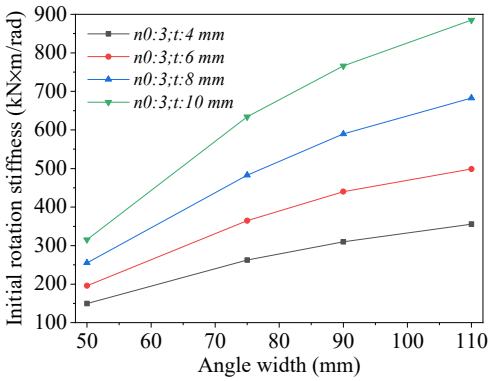

Figure 10. Effect of angle steel size on initial rotation stiffness.

Similarly, increasing the thickness from 4 mm to 10 mm resulted in an average enhancement of stiffness 33.8% per 2 mm increment across all width configurations. This improvement is as a result of the increased compressive force exerted between the bolt and the angle steel with greater thickness, which restricts relative rotation at the interface and thereby increases initial rotational stiffness.

3.1.3. Bolt Preload

To evaluate the effect of bolt preload on the initial rotational stiffness, four comparative cases were designed and analyzed. The results are shown in Figure 11. When the quantity of bolts is three, the bolt preload was applied at levels ranging from 25% to 100%, relative

to the standard installation preload, and the initial rotation stiffness increases by 3.9%, 2.2%, and 2.1% for each 25% increase, with an average increase of 2.7%. A slight positive correlation was observed between bolt preload and initial rotational stiffness, though the overall effect was negligible. This is attributed to the rotation displacement of the angle steel in the initial stage being small, and the friction effect having a small range, so the initial rotation stiffness is less affected by bolt preload.

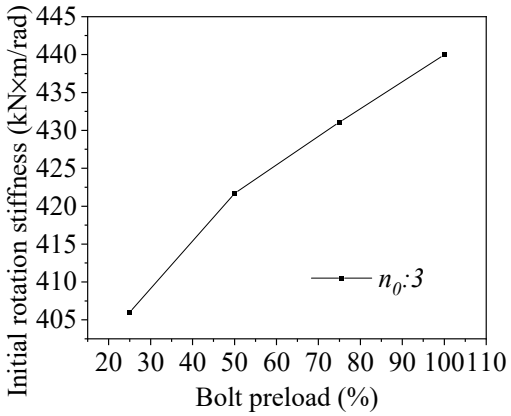

Figure 11. Effect of bolt preload on initial rotation stiffness.

3.1.4. Friction Coefficient

To evaluate the impact of the friction coefficient on initial rotational stiffness, five groups of contrast tests were designed. The results are shown in Figure 12. When the number of bolts is two, the friction coefficient increases from 0.1 to 0.5, and the initial rotation stiffness increases by 55.7%, 24.0%, 14.2%, and 9.7% for each increase of 0.1. The increased range of initial rotation stiffness decreases with increasing friction coefficient. This is attributed to the increase in the friction coefficient leading to enhanced friction between the bolt and angle steel, which leads to an increase in initial rotation stiffness, as shown in Figure 13. However, the sensitivity of the initial rotational stiffness to the friction coefficient decreases as the coefficient increases.

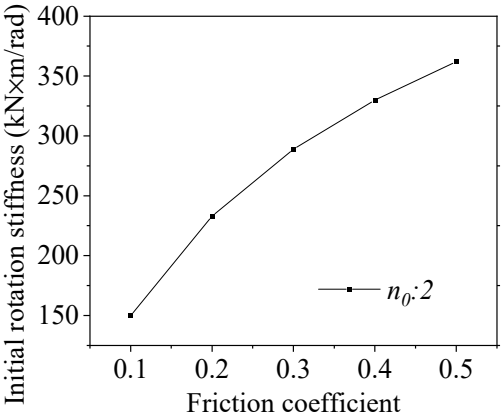

Figure 12. Effect of friction coefficient on initial rotation stiffness.

3.1.5. Number of Bolts

To investigate the effect of bolt quantity on initial rotational stiffness, eight comparative tests were conducted, with the results presented in Figure 14. For a constant angle steel width of 75 mm, each additional bolt (from one to four) increased the stiffness by 170.2, 149.1, and 136.4 kN·m/rad, respectively, averaging 151.9 kN·m/rad. Similarly, at a width

of 90 mm, the corresponding increments were 182.5, 206.9, and 184.9 kN·m/rad, with an average increase of 191.4 kN·m/rad per bolt.

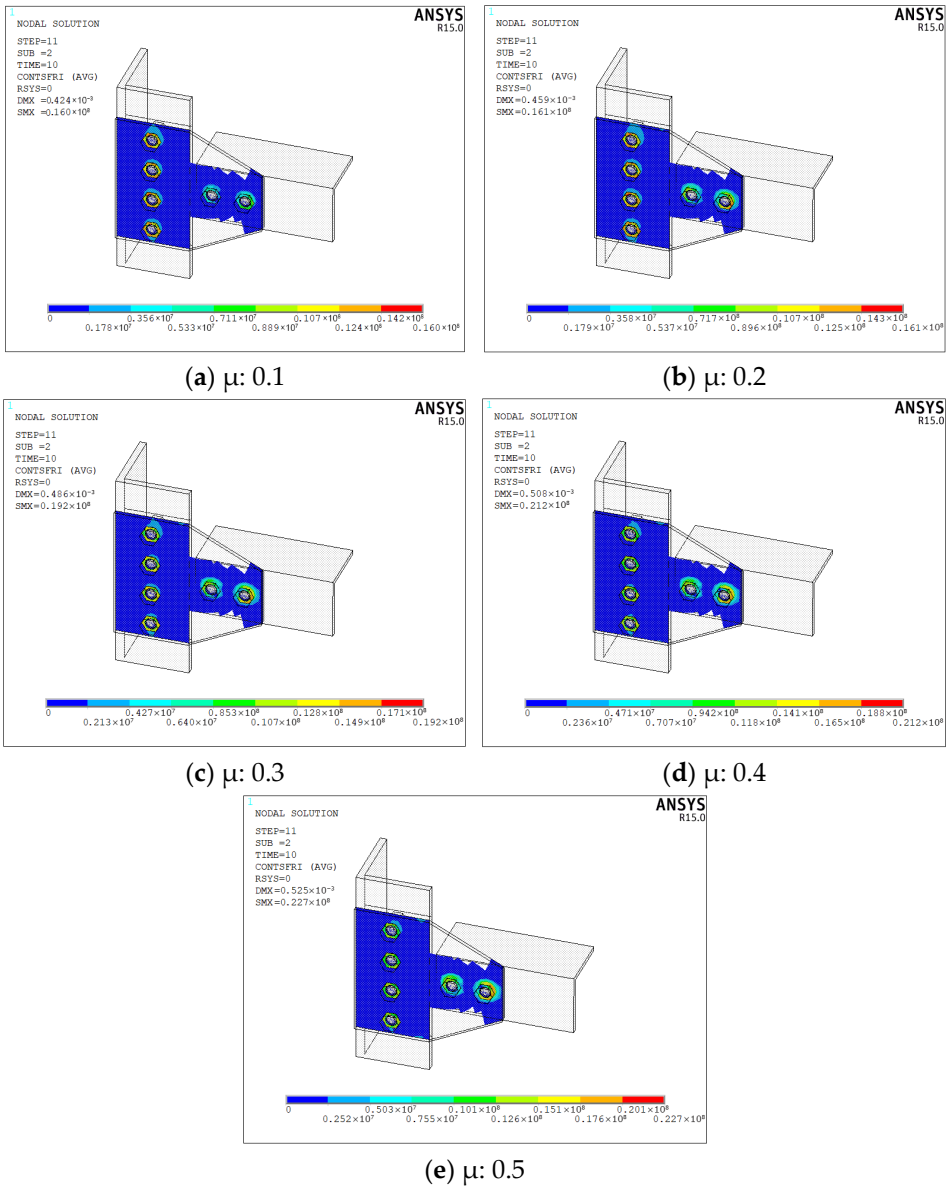

Figure 13. Friction stress cloud map of the contact pair.

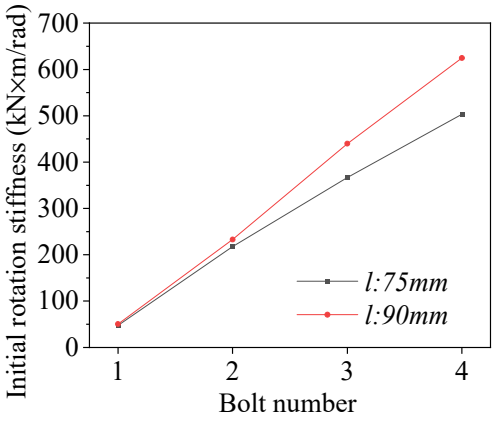

Figure 14. Effect of bolt number on initial rotation stiffness.

With different angle steel widths, the initial rotation stiffness increases approximately linearly with the increase in the quantity of bolts. This is attributed to fact that, with an increase in the number of bolts, the contact area increases exponentially, and the friction effect is enhanced, which leads to an increase in initial rotation stiffness, which can be validated from the stress cloud map in the y-direction of the joint model in Figure 15. Simultaneously, an expansion in width further enlarges the contact area, which makes the increase range of the initial rotation stiffness greater.

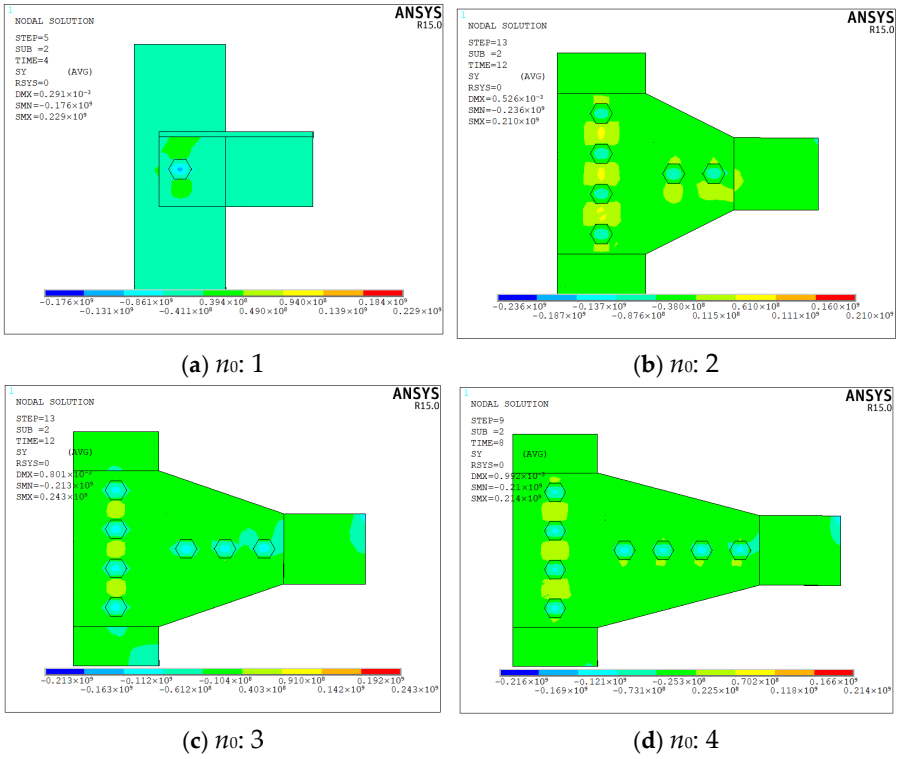

Figure 15. Stress cloud map in the y-direction of the joint model.

3.1.6. Other Influencing Factors

An additional eight comparative tests (Figure 16) revealed that the initial rotational stiffness remains largely unaffected by variations in the strength grades of the bolts and the angle steel, indicating a negligible impact of material strength on this property.

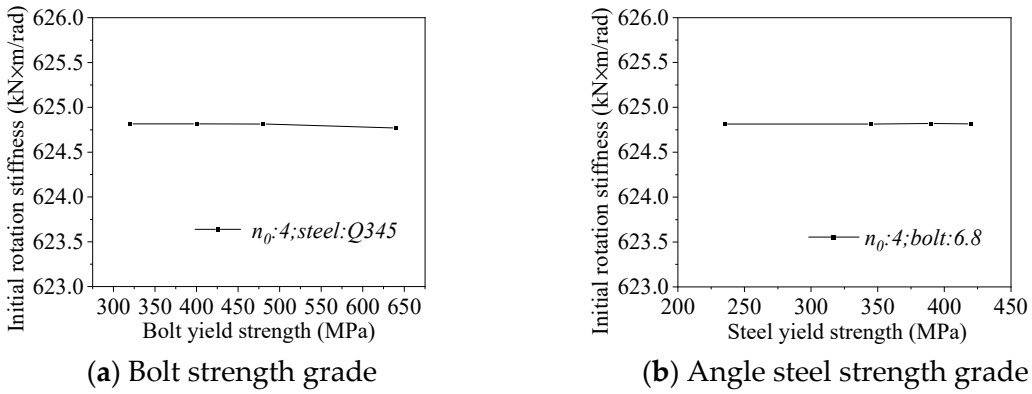

(**a**) Bolt strength grade (**b**) Angle steel strength grade

Figure 16. The influence of other factors on the initial rotation stiffness.

3.2. Factors Influencing Ultimate Bending Moment

3.2.1. Bolt Diameter

To evaluate the effect of bolt diameter on the ultimate bending moment, 31 comparative tests were conducted, with the results summarized in Figure 17. For a single-bolt configuration, increasing the bolt diameter from 12 mm to 24 mm led to an average increase in the ultimate bending moment of 86.9%, 21.0%, and 142.0% per 4 mm increment, corresponding to different angle steel thicknesses.

For the two-bolt configuration, the ultimate bending moment increased by an average of 82.4% and 20.7% per 4 mm diameter increment from 12 mm to 20 mm, across different angle steel widths. In contrast, a further diameter increase from 20 mm to 24 mm resulted in a much larger average gain of 167.4% for angle steel widths of 75, 90, and 110 mm.

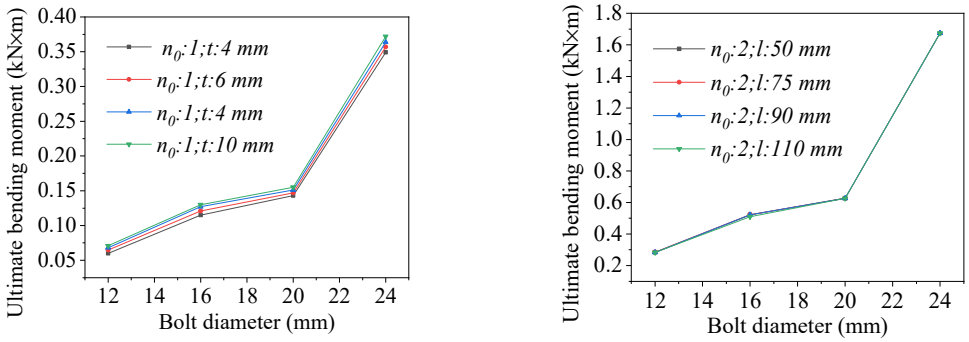

(**a**) Angle steel thickness (**b**) Angle steel width

Figure 17. Effect of bolt diameter on ultimate bending moment.

With an increase of bolt diameter, the range of the ultimate bending moment increases first, then decreases and increases sharply. An increase in the bolt diameter results in a corresponding increase in the pitch of the bolt, which will cause the moment arm of the frictional resistance to increase. The bolt preload will also increase, and the contact area increases at the same time, which will enhance the friction effect.

3.2.2. Bolt Preload

The effect of bolt preload on the ultimate bending moment was investigated through four comparative tests (Figure 18). For a three-bolt configuration, each 25% increment in preload (from 25% to 100% of the installation value) consistently enhanced the ultimate moment by 0.29, 0.284, and 0.262 kN·m, revealing a linear relationship. This trend is attributed to the increased frictional resistance at the bolt-angle steel interface under higher preloads, which impedes relative displacement, as shown in Figure 19.

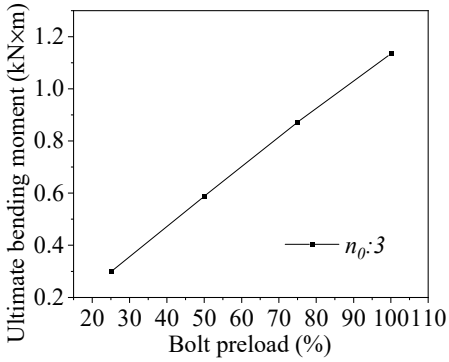

Figure 18. Effect of bolt preload on ultimate bending moment.

3.2.3. Friction Coefficient

The impact of the friction coefficient on the ultimate bending moment was examined through five comparative tests, with the results presented in Figure 20. For a two-bolt configuration, each increment of 0.1 in the friction coefficient led to an average increase in the ultimate bending moment of approximately 0.25 kN·m, demonstrating a clear linear relationship. This trend is attributed to the enhanced interfacial friction at the bolt-to-steel interfaces, which strengthens the resistance against relative displacement and thereby elevates the joint's ultimate bending capacity.

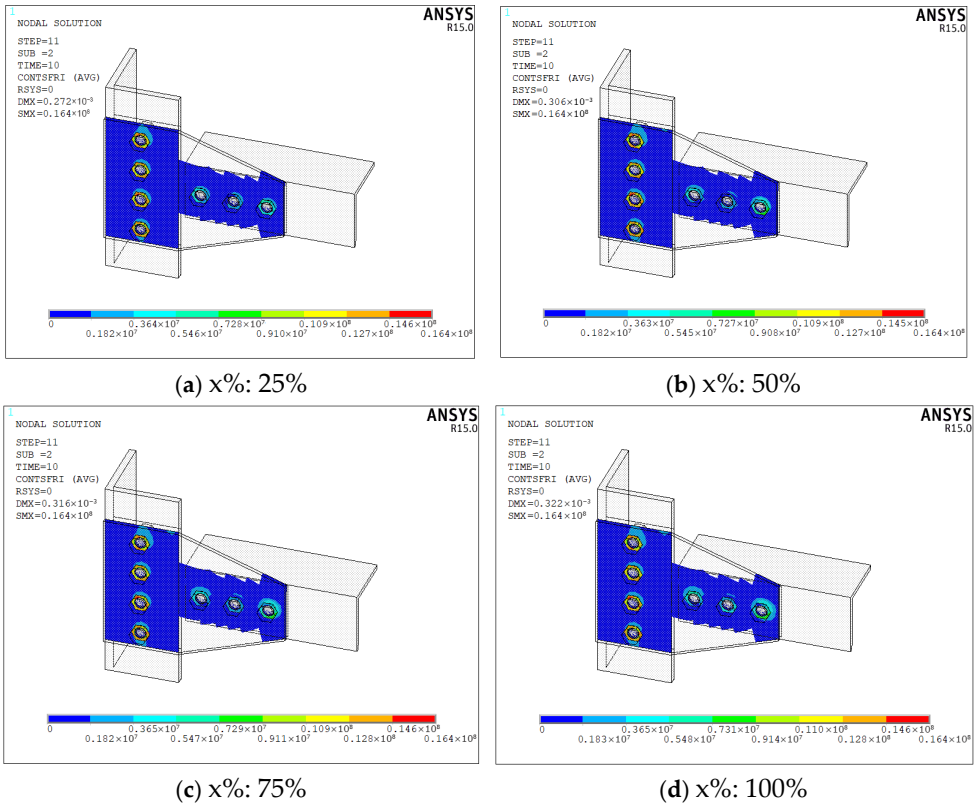

Figure 19. Friction stress cloud maps of contact pairs.

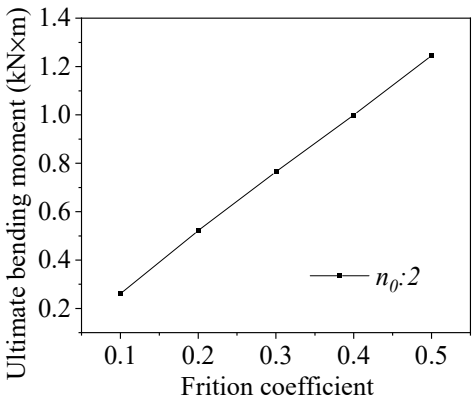

Figure 20. Effect of friction coefficient on ultimate bending moment.

3.2.4. Number of Bolts

To investigate the impact exerted by the quantity of bolts on the ultimate bending moment, eight sets of contrast tests were designed, and the results were compared in Figure 21. With different angle steel widths, as the number of bolts increases from one to

four, the ultimate bending moment increases by 0.401 kN·m, 0.612 kN·m, and 1.057 kN·m on average for every increase of one.

With the increase in the number of bolts, the increase in the range of ultimate bending moment increases gradually. This is ascribed to that fact that, as the quantity of bolts increases, the moment arm of the frictional resistance at the interface of the rotation center increases, and the friction effect is enhanced with the increase in contact area, which can be validated from friction stress cloud map of contact pairs shown in Figure 22. Finally, the friction resistance moment of the bolt to the angle steel increases in multiples at the same time.

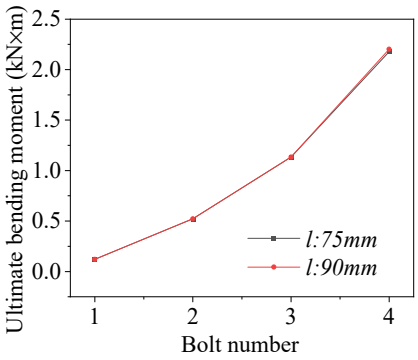

Figure 21. Effect of bolt number on ultimate bending moment.

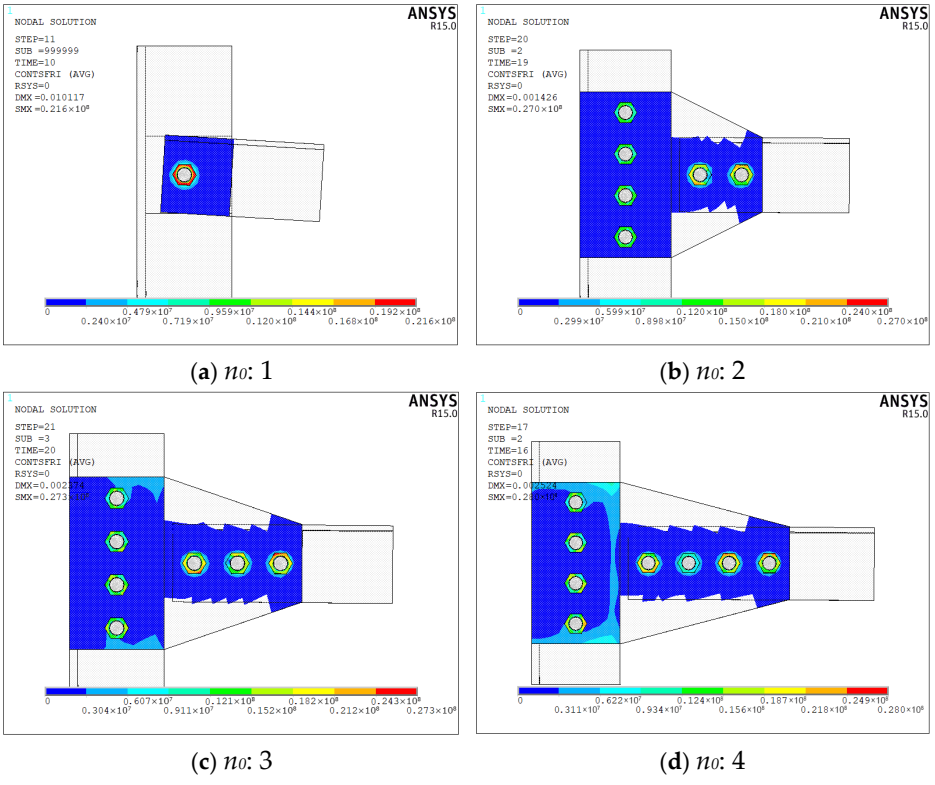

Figure 22. Friction stress cloud map of contact pairs.

3.2.5. Other Influencing Factors

Next, 24 comparative tests were conducted to investigate the influence of other factors on the ultimate bending moment, with the results summarized in Figure 23. The data demonstrate negligible sensitivity of the ultimate bending moment to increases in the yield strength of the bolt and angle steel materials in a four-bolt configuration, as well as to variations in the thickness and width in a three-bolt configuration. Therefore, the influences

of material strength and angle steel geometry on the ultimate bending moment can be reasonably disregarded.

3.3. Moment-Rotation Relationship Model

The moment-rotation response of the bolted connection obtained from the finite element simulation was fitted using the Kishi-Chen power model [26], given by Equation (1). The ultimate bending moment and relative plastic rotation angle were determined directly from the curve data, while the shape coefficient (n) was calibrated by fitting the model to the simulated response. In the formula, K_i is the initial rotation stiffness.

$$M = \frac{K_i \theta}{\left[1 + \left(\frac{\theta}{\theta_0}\right)^n\right]^{\frac{1}{n}}} \quad (1)$$

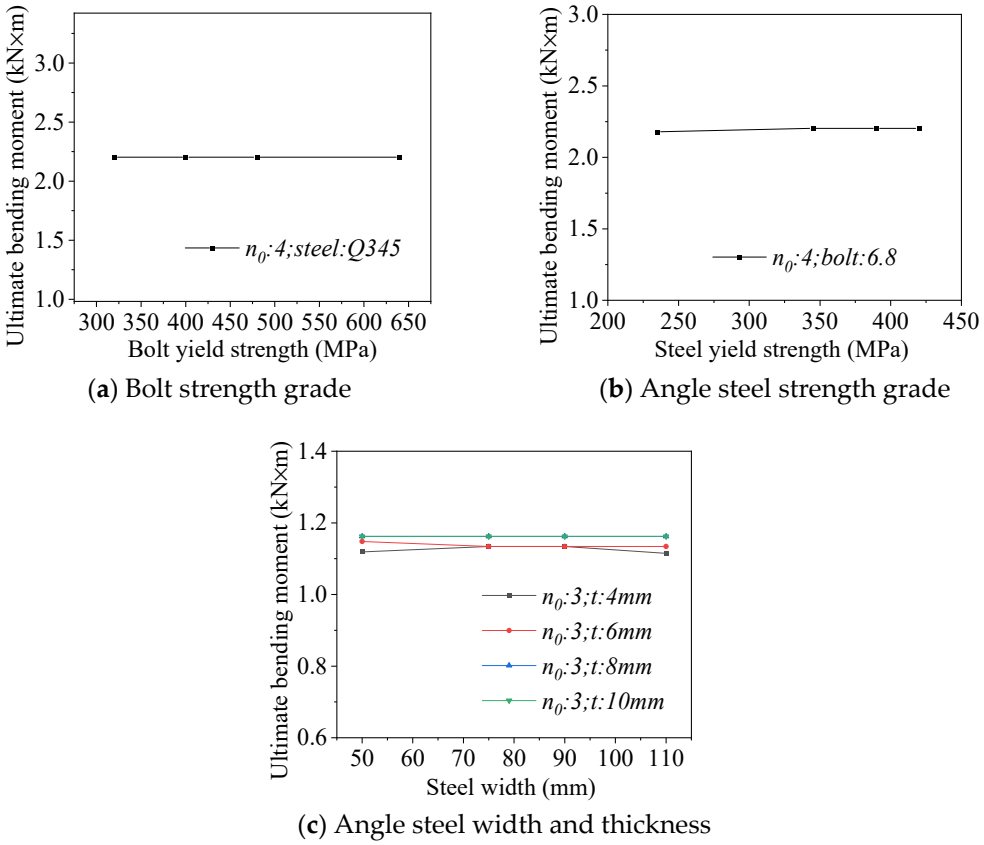

(**a**) Bolt strength grade (**b**) Angle steel strength grade

(**c**) Angle steel width and thickness

Figure 23. Effect of other factors on ultimate bending moment.

The relative plastic rotation angle θ_0 can be calculated from the initial rotation stiffness K_i and the ultimate bending moment M_u, as shown in Formula (2).

$$\theta_0 = \frac{M_u}{K_i} \quad (2)$$

According to the results described in Section 2.1, the bolt diameter d, the angle steel width l, the angle steel thickness t, the number of bolts n_0, and the friction coefficient μ are selected as the main factors influencing the initial rotation stiffness K_i. Therefore, based on the parameter analysis, a power function form was used to calculate the initial rotation stiffness K_i through data fitting, as shown in Formula (3). The mean discrepancy between the outcomes of the numerical simulations and those derived from the analytical expression for the initial rotational stiffness K_i is 2.7%. Figure 24 presents the error analysis of the

calculation for initial rotation stiffness K_i. All data points fall near the straight line y = x, and most of them are within a 20% error range. The error between the calculation results and the numerical simulation results is within the acceptable range.

$$K_i = (-0.004 + 0.006n_0)d^{1.6}l^{1.05}t^{1.03}\mu^{0.45} \quad (3)$$

According to the results described in Section 2.2, the ultimate bending moment M_u is related to the friction coefficient μ, the bolt preload F_T, and the number of bolts n_0, and the bolted connection joint is in the frictional sliding state in the ultimate state. Therefore, according to the moment balance relationship of the model, the ultimate bending moment load Mu can be calculated, as shown in Formula (4). The mean discrepancy between the outcomes of the numerical simulations and the results derived from the analytical expression for the ultimate bending moment load M_u is 6.8%. Figure 25 presents the error analysis of the calculation expression for the ultimate bending moment load M_u. It can be observed that all data points fall near the straight line y = x, and most of them are within a 15% error range.

$$M_u = \sum_{i=1}^{n_0}(2F_T\mu L)_i \quad (4)$$

In the formula, μ is the friction coefficient, F_T is the bolt preload, n_0 is the number of bolts, and L is the moment arm value of the friction to the rotation center of the bolted joint model.

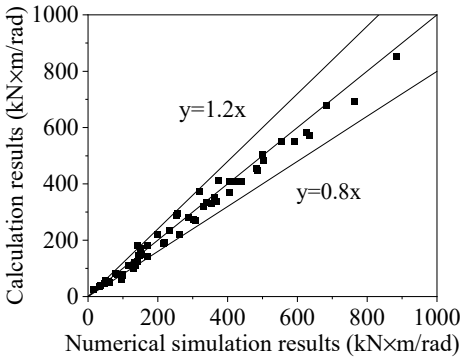

Figure 24. Error analysis of initial rotation stiffness.

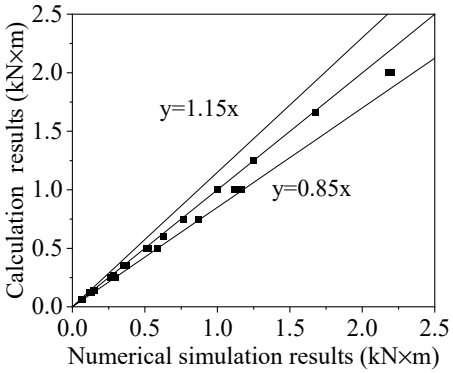

Figure 25. Error analysis of ultimate bending moment.

The blot quantity n_0, the bolt diameter d, the angle steel width l, the angle steel thickness t, and the bolt preload x% are selected as variables, and the shape coefficient n is calculated by data fitting in the form of a power function, as shown in Formula (5). The mean discrepancy between the outcomes of the numerical simulations and those derived from analysis of the shape coefficient n is 0.7%. Figure 26 presents the error analysis of the

calculation results for the shape coefficient n. It can be observed that all data points fall near the straight line y = x, and most of them are within a 20% error range. The error between the calculation results and the numerical simulation results is within the acceptable range.

$$n = 1.14 \frac{{n_0}^{0.52} d^{0.6} x\%^{0.1}}{l^{0.16} t^{0.44}} \quad (5)$$

In the formula, l is the width, d is the diameter, t is the angle steel thickness, n_0 is the number of bolts, and $x\%$ is the bolt preload.

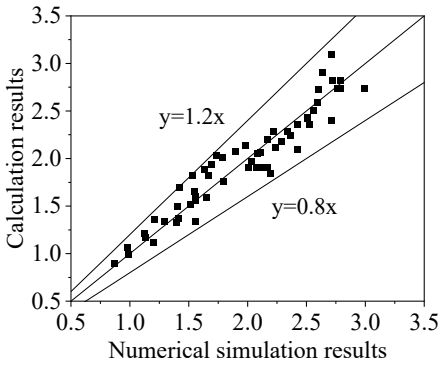

Figure 26. Error analysis of shape coefficient.

Among the parameters in the above calculation expression, the length unit is mm, the rotation angle unit is rad, the load unit is kN, the bending moment unit is kN × m, and the initial rotation stiffness unit is kN × m/rad. The bolt number value range is one to four, the bolt grade is 4.8 to 8.8, the steel grade is Q235 to Q420, the bolt diameter is 12 to 24 mm, the steel thickness is 4 to 10 mm, the steel width is 50 to110 mm, and the friction coefficient is 0.1 to 0.5.

Based on the established bending moment-rotation curve model, when parameters such as bolt quantity, angle steel width and thickness, bolt diameter, and friction coefficient are available, the bending moment-rotation model of the bolted joint in the range of contact friction can be obtained.

The bending moment-rotation model proposed in this paper provides a model for semi-rigid analysis of bolted joint structures. Existing semi-rigid-related models, such as the Kishi-Chen model [2], the Richard-Abbott model, and the Ramberg-Osgood model [3], are suitable for semi-rigid steel frame beam-column joints, which are different from the model proposed for bolted joints in this paper. Future studies should verify of the accuracy and reliability of the moment-rotation model and investigate related engineering applications.

4. Conclusions

In this study, a finite element model of bolted steel connections has been developed and experimentally validated. The influence of eight parameters encompassing bolt configuration (number, diameter, preload), material properties (bolt and grade of angle steel), geometry (angle steel width and thickness), and interfacial condition (friction coefficient) on joint semi-rigidity is thoroughly investigated. A generalized moment-rotation model for the connection is subsequently derived. The key conclusions are as follows:

(1) The primary factors influencing the initial rotational stiffness of the bolted joint are the bolt diameter, the width and thickness of the angle steel, the bolt preload, the friction coefficient, and the quantity of bolts. In contrast, the strength grades of both the bolt and the angle steel have minimal impact. Notably, the stiffness demonstrated an average increase of 50.6% per 4 mm increment as the diameter of the bolt increased

from 12 mm to 24 mm. Furthermore, expanding the width from 50 to 75 mm resulted in a substantial average increase of 88.5% in the initial rotational stiffness. For angle steel widths increasing from 75 mm to 110 mm, the initial rotation stiffness increases by 17.4% on average for every 17.5 mm increase. The initial rotation stiffness increases by 33.8% on average for every 2 mm increase in angle steel thickness from 4 mm to 10 mm. As the friction coefficient increases, the range of initial rotation stiffness decreases. The initial rotation stiffness increases approximately linearly with an increase in the number of bolts.

(2) Bolt diameter, preload, friction coefficient, and number of bolts have a strong influence on the ultimate bending moment of the bolted joint, while bolt strength, angle steel strength, angle steel width, and angle steel thickness have little effect. As the bolt diameter increases, the range of ultimate bending moment increases first, then decreases and increases sharply. The ultimate bending moment exhibits a linear correlation with both bolt preload and friction coefficient. Furthermore, it increases progressively with the number of bolts, demonstrating a more pronounced enhancement.

(3) According to the analysis of different of bolted joint parameters, the moment-rotation curve model of semi-rigid joints is established by fitting, using the power function model proposed by Kishi-Chen [2] et al., and it can be used for mechanical performance analysis of semi-rigid steel structure joints with bolted connection.

Author Contributions: M.K.: supervision, investigation, methodology, writing—review and editing; S.H.: data curation, investigation, formal analysis, writing—original draft; J.C.: formal analysis, writing—review and editing; L.Z.: investigation. All authors have read and agreed to the published version of the manuscript.

Funding: This work is funded by the Jilin Provincial Science and Technology Development Plan Project—Young and Middle-aged Scientific and Technological Innovation Talent (Team) Project (No. 20250601091RC), Jilin Provincial Department of Science and Technology.

Data Availability Statement: The dataset is available upon request from the authors.

Conflicts of Interest: Author Shifeng Hou was employed by the company Guangdong Power Grid Co., Ltd. Author Liang Zhang was employed by the company Economic and Technical Research Institute of State Grid Henan Electric Power Company. The remaining authors declare that the research was conducted in the absence of any commercial or financial relationships that could be construed as a potential conflict of interest.

References

1. Faella, C.; Piluso, V.; Rizzano, G. *Structural Steel Semirigid Connections: Theory, Design and Software*; CRC Press: Boca Raton, FL, USA, 2000.
2. Chen, W.F.; Kishi, N. Semirigid Steel Beam-to-Column Connections: Data Base and Modeling. *J. Struct. Eng.* **1989**, *115*, 105–119. [CrossRef]
3. Attiogbe, E.; Morris, G. Moment-Rotation Functions for Steel Connections. *J. Struct. Eng.* **1991**, *117*, 1703–1718. [CrossRef]
4. Reza, A.; Akbar, P. Nonlinear analysis of damped semi-rigid frames considering moment–shear interaction of connections. *Int. J. Mech. Sci.* **2014**, *81*, 165–173. [CrossRef]
5. Thai, H.; Uy, B.; Kang, W.; Hicks, S. System reliability evaluation of steel frames with semi-rigid connections. *J. Constr. Steel Res.* **2016**, *121*, 29–39. [CrossRef]
6. Yu, Y.; Zhu, X. Nonlinear dynamic collapse analysis of semi-rigid steel frames based on the finite particle method. *Eng. Struct.* **2016**, *118*, 383–393. [CrossRef]
7. Zhao, B.D.; Chen, Y.; Liu, C.Q.; Wu, H.D.; Wang, T.; Wei, X.D. An axial semi-rigid connection model for cross-type transverse branch plate-to-CHS joints (Article). *Eng. Struct.* **2019**, *181*, 413–426. [CrossRef]
8. Mokhtar, R.; Ibrahim, Z.; Jumaat, M.Z.; Hamid, Z.A.; Rahim, A.H.A. Behaviour of semi-rigid precast beam-to-column connection determined using static and reversible load tests. *Meas. J. Int. Meas. Confed.* **2020**, *164*, 108007. [CrossRef]
9. Ding, J.M.; Shen, Z.Y. Influence of semi-rigid joints on internal force and displacement of steel frame structure. *Build. Struct.* **1991**, *6*, 8–12. [CrossRef]

10. Ma, H.; Yu, Z.; Zhao, Y.; Fan, F. Behavior of HCR semi-rigid joints under complex loads and its effect on stability of steel cooling towers. *Eng. Struct.* **2020**, *222*, 111062. [CrossRef]
11. Celik, H.K.; Sakar, G. Semi-Rigid connections in steel structures State-of-the-Art report on modelling, analysis and design. *Steel Compos. Struct.* **2022**, *45*, 1–21. [CrossRef]
12. Pan, J.; Yang, Z.; Wang, Z.; Dong, X. Numerical analysis of seismic performance of semi-rigid composite frame based on multi-scale. *J. Tianjin Univ. (Nat. Sci. Eng. Technol. Ed.)* **2016**, *49*, 161–167. (In Chinese) [CrossRef]
13. Kang, Z.; Wang, S.; Du, X.; Zhang, S. Research on mechanical properties of semi-rigid beam-column joints with T-shaped steel connections. *J. Build. Struct.* **2020**, *41*, 44–54. [CrossRef]
14. Zhai, X.; Zha, X.; Wang, K.; Wang, H. Initial lateral stiffness of plate-type modular steel frame structure with semi-rigid corner connections. *Structures* **2023**, *56*, 105021. [CrossRef]
15. Nguyen, T.D.; Vu, Q.A. Analysis of steel frame with semi-rigid connections and constraints using a condensed finite element formulation. *Int. J. GEOMATE* **2023**, *25*, 113–121. [CrossRef]
16. Qiu, F.; Qiu, J.; Feng, H.; Wang, H.; Qian, H.; Jin, X.; Wang, K.; Fan, F. Calculation method of stability bearing capacity of transmission tower angle steel considering semi-rigid constraint. *Curved Layer. Struct.* **2022**, *9*, 202–211. [CrossRef]
17. Tang, Z.; Li, Z.; Wang, T. Direct Prediction Method for Semi-Rigid Behavior of K-Joint in Transmission Towers Based on Surrogate Model. *Int. J. Struct. Stab. Dyn.* **2023**, *23*, 2350027. [CrossRef]
18. Tang, Z.; Li, Z.; Wang, T. GPR-based prediction and uncertainty quantification for bearing capacity of steel tubular members considering semi-rigid connections in transmission towers. *Eng. Fail. Anal.* **2022**, *142*, 106854. [CrossRef]
19. Tang, Z.; Li, Z.; Wang, T.; Lu, D.; Tan, Y. PDEM-based multi-component and global reliability evaluation framework for steel tubular transmission towers with semi-rigid connections. *Eng. Struct.* **2023**, *295*, 116838. [CrossRef]
20. Al-Sherif, R.H.; Ismael, M.A. Effect of Semi-Rigid Beam-Column Connection on Structural Behavior of Steel Frames. *Fourth Int. Conf. Civ. Environ. Eng. Technol. AIP Conf. Proc.* **2023**, *2775*, 020008-1–020008-19. [CrossRef]
21. Tang, Z.; Wang, T.; Li, Z. Probabilistic bearing capacity assessment for cross-bracings with semi-rigid connections in transmission towers. *Struct. Eng. Mech.* **2024**, *89*, 309–321.
22. Sun, D. Research on the Mechanical Calculation Model of Transmission Line Tower in Mining Area and the Interaction Mechanism of Tower-Line System. Doctoral Dissertation, China University of Mining and Technology, Xuzhou, China, 2010.
23. *BS EN 10027-1:2016*; Designation Systems for Steels—Steel Names. European Committee for Standardization (CEN): Brussels, Belgium, 2016. [CrossRef]
24. *EN 1993—1–8*; Eurocode 3, Design of Steel Structures, Part 1–8: Design of Joints. European Committee for Standardization (CEN): Brussels, Belgium, 2005.
25. *GB 50017—2017*; Standard for Design of Steel Structures. Ministry of Housing and Urban-Rural Development of the People's Republic of China: Beijing, China; Architecture & Building Press: Beijing, China, 2017.
26. Kishi, N.; Chen, W.-F. Moment-rotation relations of semirigid connections with angles. *J. Struct. Eng.* **1990**, *116*, 1813–1834. [CrossRef]

Disclaimer/Publisher's Note: The statements, opinions and data contained in all publications are solely those of the individual author(s) and contributor(s) and not of MDPI and/or the editor(s). MDPI and/or the editor(s) disclaim responsibility for any injury to people or property resulting from any ideas, methods, instructions or products referred to in the content.